lubricants

MDPI

Article

Effect of CH_4 Flow Rate on the Tribological Behaviors of TiCN Films against Si_3N_4 Ceramic and Steel Ball

Yanhong Lyu [1,*], Jianyun Zheng [2], Huilian Sun [1], Xinrong Deng [1], Yang Liu [1] and Qiaoyu Zhang [1]

[1] School of Physical and Chemistry, Hunan First Normal University, Changsha 410205, China
[2] State Key Laboratory of Solid Lubrication, Lanzhou Institute of Chemical Physics, Chinese Academy of Sciences, Lanzhou 730000, China
* Correspondence: lyh@hnfnu.edu.cn

Abstract: Control of the structural, mechanical and tribological properties of TiCN films play an important role in its numerous applications, including the cutting tools, mechanical components, aeronautical and biomedical engineering industries. Direct-current magnetron sputtering (DCMS) system was applied to deposit TiCN films onto n-type silicon (100) at room temperature. The Ti-TiN interlayer was used to enhance the adhesive strength between the coating and the substrate. The composition and microstructure of the TiCN films were studied using X-ray photoelectron spectroscopy (XPS) and field-emitted scanning electron microscopy (FESEM). The mechanical properties of the films as a function of methane (CH_4) flow ratio were then characterized using nano-indentation measurements. The tribological behavior of TiCN films was investigated by UMT-2MT tribometer against a Si_3N_4 ceramic and AISI52100 steel ball. After the tribological tests, the wear rate of the films was obtained by the 3D surface profiler and the component content of wear debris was evaluated by energy dispersive X-ray spectroscopy (EDS). The results show that the tribological properties of TiCN films are a function of CH_4 flow rates. The film obtained at a 10 sccm CH_4 flow rate possesses a minimum average COF value of 0.1964 and reaches 72,000 cycles against a Si_3N_4 ball over the test duration. Furthermore, the wear rate was only 2.076×10^{-6} mm^3/N·m. Furthermore, the TiCN films exhibited longer lifespan against the Si_3N_4 ball than against the steel ball under the normal load of 1 N, indicating that the TiCN films present better lubricative properties when against low-hardness counterparts than high-hardness counterparts.

Keywords: TiCN film; direct-current magnetron sputtering; CH_4 flow rate; tribological behavior

check for updates

Citation: Lyu, Y.; Zheng, J.; Sun, H.; Deng, X.; Liu, Y.; Zhang, Q. Effect of CH_4 Flow Rate on the Tribological Behaviors of TiCN Films against Si_3N_4 Ceramic and Steel Ball. *Lubricants* **2023**, *11*, 209. https://doi.org/10.3390/lubricants11050209

Received: 19 April 2023
Revised: 26 April 2023
Accepted: 27 April 2023
Published: 8 May 2023

1. Introduction

Tool wear, including crater wear, nose wear, fracture wear and flank wear, are destructive and determine the tool's life [1]. Surface modification, such as hard film deposition, is a responsible way to enhance the tool's service life. In general, the wear resistance and optimized mechanical properties of hard films depend on grain size, chemical composition, hardness, surface stress and so on, which are highly related to preparation parameters, including deposition temperature, bias voltage, current density, gas flow rate, etc. Furthermore, the friction environment and friction medium also strongly affect the tribological properties of the films [2,3].

Early, hard films have been deposited by the CVD method at a high deposition temperature (1000 °C) [4]. In order to reduce the deposition temperature, various PVD techniques, including magnetron sputtering [5–7], laser ablation [8], cathodic arc [9] and plasma immersion ion implantation [10], have been developed. Among them, magnetron sputtering technology is the most attractive due to the high deposition rate, high ionization rate, stable sputtering reaction and low deposition temperatures [11–14]. Compared to other magnetron sputtering methods, direct-current magnetron sputtering (DCMS) has higher sputtering and film deposition rates and can be effectively control the stoichiometric ratio of film when the pure metal target and appropriate amount of reactive gas (such as O_2, N_2, etc.) added into the working gas (such as argon) are used for sputtering.

Several studies that focus on hard films have been reported. Among them, TiN and TiCN films have been used extensively as protective layers because of their high hardness, chemical stability and better wear resistance [15,16]. TiN is widely used in various tribological applications, but its performance is limited at high temperatures (≥600 °C) [17]. TiCN exhibits higher hardness and better resistance to oxidation at high temperatures compared to TiN because it combines the advantages of TiN and TiC [5]. In recent years, owing to its better oxidation resistance and high hardness, TiCN has gained wide attention by researchers. Cheng Y.H. et al. have studied the influence of CH_4 contents on the composition, structure and internal stress of TiCN films deposited by the large-area filtered-arc deposition (LAFAD) technique [4]. Compared to monolayer films, multilayer films exhibit much more excellent mechanical and tribological properties. Su Y.L. and Kao W.H. researched the tribological behavior and wear mechanisms of TiN-TiCN-TiN multilayer films [18]. Yang Y.L. et al. reported the phase constituents and mechanical properties TiCN/TiN films synthesized by laser in situ [15].

It is documented that PVD TiCN films are applied as protective films for cutting tools, automobile parts and biomedical instrumentation [19–22]. However, in order to obtain high-quality hard films and expand the application range, the relationship between the preparation parameters, the friction medium and the properties of the TiCN-based multilayer films should be further studied. In this paper, we deposited Ti/TiN/TiCN triple-layer films by DCMS and investigated the microstructure, mechanical properties and tribological behaviors of the top layer of TiCN films. It was found that the tribological behaviors of TiCN films against steel and Si_3N_4 balls are closely related to the microstructure and mechanical properties determined by CH_4 flow rate, and the optimal tribological behavior of films against steel and Si_3N_4 balls was obtained.

2. Materials and Methods

2.1. Film Deposition

n-type Si (100) wafers with a surface roughness of 20 nm and stainless steel (1Cr18Mn8Ni5N) were used as the substrate materials. The films were deposited by DC reactive-magnetron-sputtering titanium target (purity > 99.5 wt.%) at room temperature. The working gas and reactive gas were Argon (Ar) gas, nitrogen (N_2) gas and the mixed gas of nitrogen (N_2) and methane (CH_4). The purity of gases used were 99.99%. The schematic diagram of the deposition system is shown in Figure 1. All of the substrates were ultrasonically cleaned in ethyl alcohol and acetone for 10 min before deposition. The distance between the substrate and the target was controlled to 10 cm. The system was evacuated to a base pressure under 7×10^{-4} Pa before deposition. Prior to deposition, the substrates were cleaned by argon plasma bombardment for 10 min to remove any residual contaminants on the surfaces. After that, a Ti layer was deposited in a pure Ar atmosphere with 20 sccm. Then, the TiN layer was deposited under a 2.0 direct current for 25 min in mixed gas of Ar (20 sccm) and N_2 (6 sccm). Following this, the TiCN film was obtained in a gaseous mixture of CH_4 (3, 5, 8, 10, and 12 sccm) and N_2 (6 sccm) for 25 min. During deposition, a bias voltage of −100 V and duty cycle of 80% was applied to the substrates.

2.2. Film Characterization

Conventional Bragg–Brentano X-ray diffraction (XRD) using a Philips X'Pert-MRD type diffractometer with a Cu tube operated at 40 kV and 60 mA was performed to study the crystalline structure and calculate the grain size in the films. The morphologies of the fractured cross-section and surface of the films were observed using FESEM (JSM-6701F). The composition of the films was analyzed by XPS with monochromated Al Kα radiation at a pass energy of 29.4 eV. The microstructure of the films was also demonstrated by a HR800 Raman microscope with a 532 nm Ar ion laser and a resolution of 1 cm^{-1}. The hardness of the films was determined using a nano-indenter (Nanotest 600) with a Berkovich diamond tip. The indentation depth was about 10% of the film thickness in order to reduce the influence of substrates [9]. Five replicate indentations were made for each sample and the hardness was calculated from the loading–unloading curves.

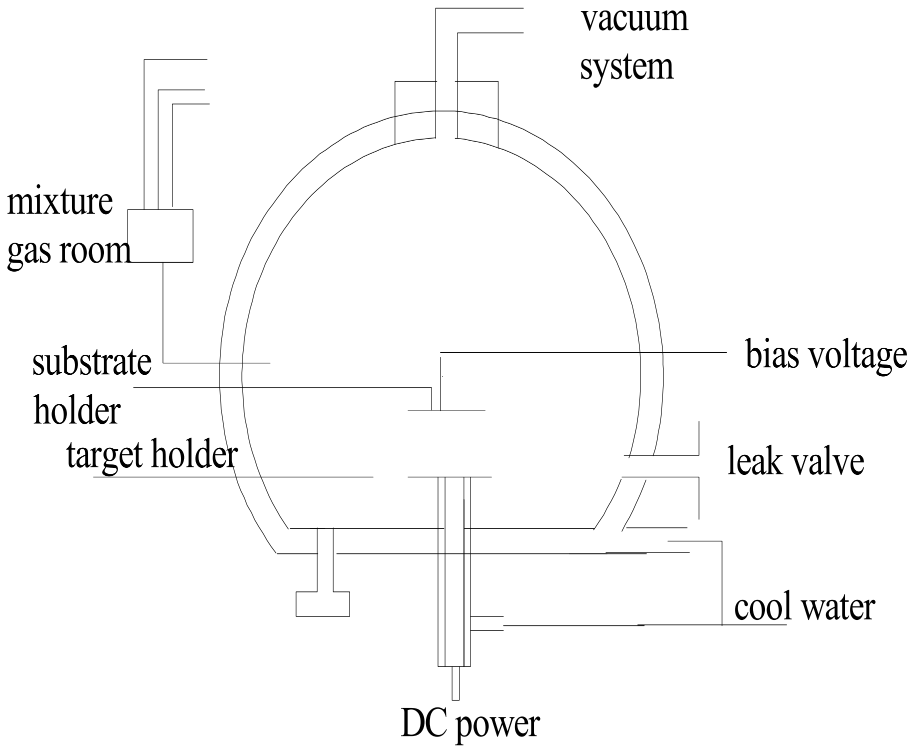

Figure 1. Top view of the DCMS deposition system.

2.3. Tribological Tests

The tribological behavior of the films was evaluated by UMT-2MT tribometer using the counterparts of the AISI52100 steel ball and the Si_3N_4 ball at a room temperature of about 25 °C and a humidity of 47%. The diameter and surface roughness of the AISI52100 steel and Si_3N_4 ball were 3 mm and 0.02 µm, and their hardness was 850 HV and 1600 HV, respectively. All the tests were conducted at a sliding speed of 600 rpm and a load of 1 N. The sliding stroke was about 5 mm. The wear volume was measured using Micro XAM-3D Surface Profile. The wear rate was calculated from the wear volume. The components of wear debris were analyzed by energy dispersive X-ray spectroscopy (EDS) in a scanning electron microscope (SEM).

3. Results

3.1. Composition and Microstructure

The XPS results of the deposited films under various CH_4 flow rates are given in Table 1. It can be found that the ratio of Ti and N decreased as the CH_4 flow rates increased, while C firstly enhanced and was then stationary. In general, by adding CH_4 gas, the concentration of C ions rises, which induces the dilution of the whole plasma. In addition, the reactivity between Ti and N ions decreased in the plasma because C ions participate in the reaction of the Ti ions, so the N ions reduced. In addition, the increase in CH_4 gas molecules also led to the Ti atom suffering from higher scattering in the collisions [8], which is the main reason for the decrease in Ti ions. However, the increase in C can form the TiC phase inlaid in the TiN plane or amorphous carbon located at the border of the TiN crystal. Furthermore, O abruptly dropped and was then an invariable trend. It should be noted that O was not deliberately introduced, and its presence was attributed to the exposure in the air, resulting in the spontaneous oxidation process of Ti [19]. When the TiCN films were deposited under CH_4 flow rates of 8 sccm, the C relative contents increased drastically and the Ti, N and O relative contents decreased obviously. This could be attributed to the films producing a dense microstructure. Therefore, the microstructure of TiCN films has been further confirmed by XRD analysis, Raman spectra and FESEM measurements.

Table 1. Composition of the films' surface measured by XPS.

CH_4 (sccm)	Ti (at.%)	C (at.%)	N (at.%)	O (at.%)
3	26.70	29.05	22.95	21.30
5	21.49	37.17	20.08	21.26
8	11.69	65.75	10.79	11.77
10	9.28	69.96	7.66	13.10
12	7.32	70.42	10.13	12.13

The XRD patterns of the TiCN films with various CH_4 flow rates from 5 to 12 sccm are given in Figure 2. The results indicate that the CH_4 flow rate has a significant influence on the grain size, phase structure and preferred orientation of the TiCN films. In Figure 2, the films deposited at high CH_4 flow rates possess a finer grain size because of the broader full width at half maximum (FWHM). As a result, the films provided with a denser microstructure increased the CH_4 flow rate. In the films deposited under 10 sccm CH_4 flow rates, the average size of crystal was about 10 nm, evaluated from the FWHM of the TiN (200) peak by the Scherrer formula. This result is in agreement with the findings of other authors [20]. It can be seen that the films presented a NaCl-type TiN polycrystalline structure. However, the films deposited at the 10 sccm CH_4 flow rates showed an obvious TiC (220) peak. It is suggested that the TiC phase is formed via local epitaxial growth on the TiN (220) plane. With increasing CH_4 flow rates, preferred orientation of the TiCN films changed from TiN (111) to (200). The grain size calculated by Scherrer's formula is shown in Figure 2b [23,24]. It is observed the grain size decreased from 19.3 nm to 4.1 nm as the CH_4 flow rate increased, which would have great influence on structural and mechanical properties.

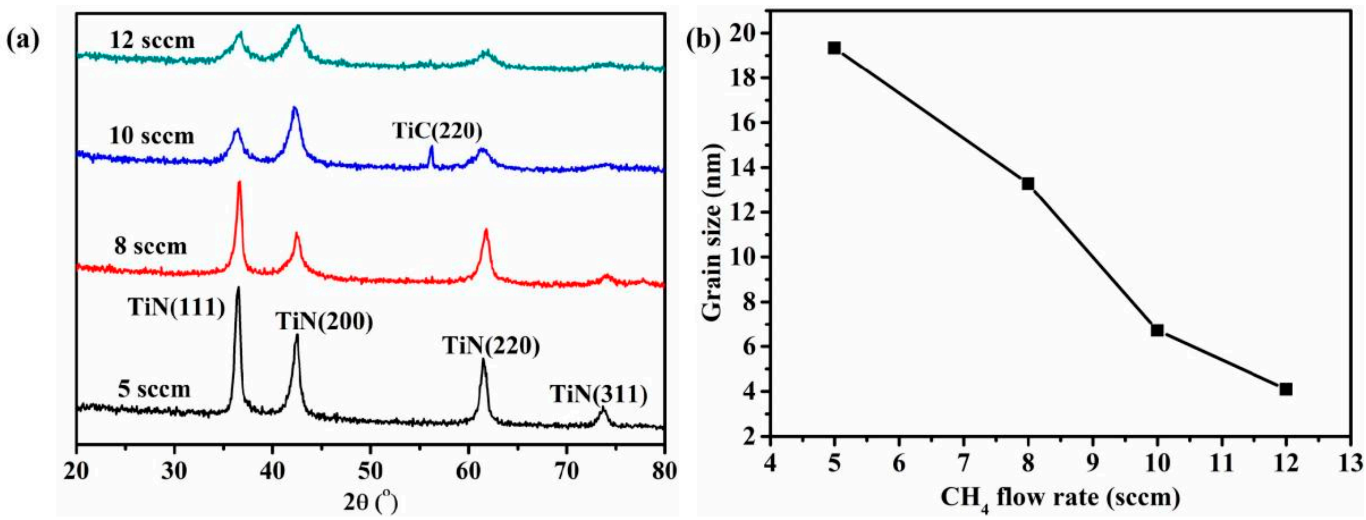

Figure 2. X-ray diffraction patterns (**a**)and grain size (**b**) of the films deposited in different CH_4 flow.

It is known that Raman can provide information about the carbon bonding configuration. Figure 3 shows the Raman spectra corresponding to the films grown at different CH_4 flow rates. The Raman shift of all spectrums ranges from 1000 to 2000 cm^{-1}. The films deposited under CH_4 flow rates from 5 to 12 sccm show the appearance of Raman signals at 1380 cm^{-1} and 1560 cm^{-1}, which is an indication of the presence of amorphous carbon [21]. This result is in agreement with the conclusion of XPS. It is also revealed that the films provide better lubricity, which is relative to the low or free C-containing films [22]. The tribological behaviors of the films are also included in Figure 4 and are be discussed later.

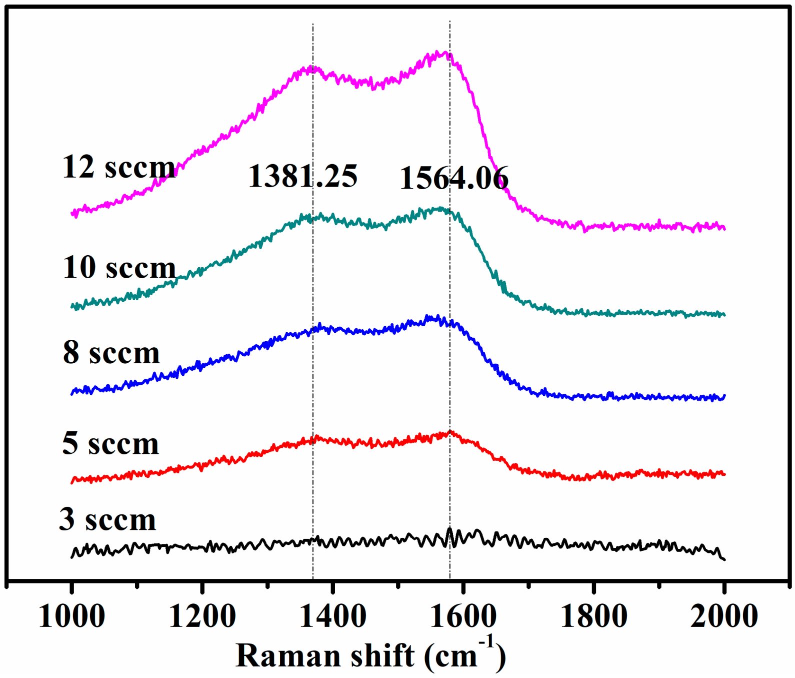

Figure 3. Raman spectra for the films deposited at different CH_4 flow rates.

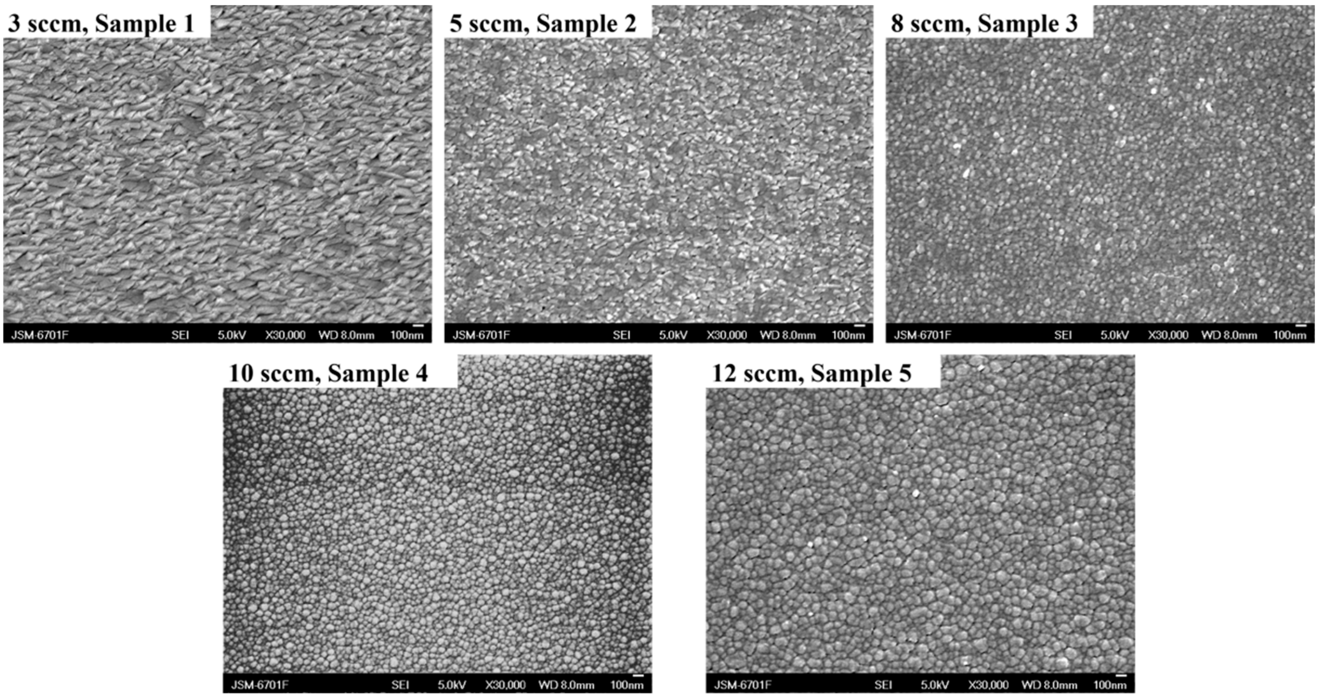

Figure 4. FESEM images of surface morphologies of the films deposited at different CH_4 flow.

The films deposited under CH_4 flow rates of 3, 5, 8, 10 and 12 sccm are referred to in sample 1 to 5, respectively. In order to acquire the microstructure information of the films, the FESEM technique was employed to observe the morphologies of the surfaces and fractured cross-section. Figure 4 shows the typical SEM images of the TiCN films' surface morphologies deposited at variable CH_4 flow rates. As described in Figure 4, an obvious evolution of microstructures from a loose and sharp pyramid-like column to a dense and globular nanostructure arises with increasing CH_4 flow rates from 3 to 12 sccm. In these photographs, the grain sizes are gradually fine with increasing CH_4 flow rates, except that of sample 5 because the C atom has a bigger radius than the N atom [4], which is in line with the XRD result. In Figure 4, it is apparently revealed that the surfaces of samples 1 and 2 consist of the pyramid-like column grains separated by pore or titanium oxide, but those of samples 3 to 5 appear to be extremely tight without titanium oxide or pores, which can be attributed to the dense microstructure at the surfaces.

Figure 5 depicts the morphologies of the fractured cross-section of the samples. It can be seen that sample 1 possesses an obvious columnar structure. However, the TiN layer from the TiCN layer can hardly be distinguished just by Figure 5a. The border of the columnar structure of pure crystalline TiN is found to severely adhere to the amorphous C phases in sample 2 observed from Figure 5b. These results further confirm the conclusion of the previous section.

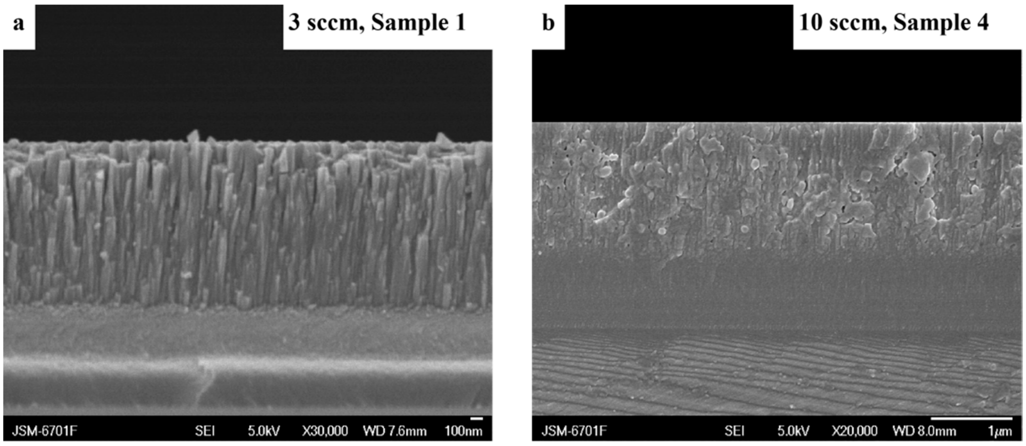

Figure 5. FESEM images of fractured cross-section of films deposited at CH_4 flow with 3 sccm (**a**) and 10 sccm (**b**).

3.2. Nanoindentation Tests

Due to the very low thickness of the single layers, we did not try to acquire values for each individual layer because very low loads lead to very high dispersions [25]. Therefore, the values of hardness in this work accord with the whole thickness of the films. Figure 6 shows the average hardness of the films deposited under different CH_4 flow rates. Generally, the hardness of films depends on many factors, such as phase composition, growth orientation, grain size, etc. Amorphous phase and low grain size are beneficial to the improvement of hardness. Regarding these aspects, sample 3 and sample 4 deposited on a CH_4 flow rate of 8 sccm and 10 sccm, respectively, own the maximum hardness value due to appropriate grain size and the formation of appropriate amount of amorphous carbon, hindering dislocation of the TiCN crystal [26].

The value of H^3/E^2 (shown in Figure 7a) that is significantly related to the wear resistance of films as a function of CH_4 flow rates is given in Figure 7. It can be found that the value of H^3/E^2 increases firstly and then decreases. It is worth noting that the ratio value of sample 4 is higher than that of other samples. The scratch test shown in Figure 7b–e exhibits that sample 4 has excellent adhesion force between the film and the substrate. These results show that sample 4 has good resistance to plastic deformation [17]. Therefore, we could conjecture that sample 4 deposited under a 10 sccm CH_4 flow rate should have the lowest wear rate. The detailed study is discussed in the subsequent section.

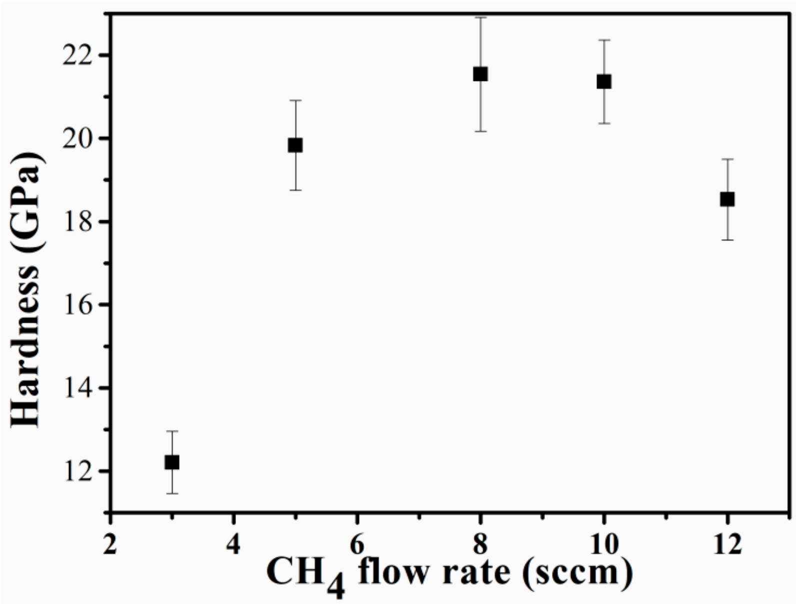

Figure 6. The average hardness of the films deposited under different CH_4 flow rates.

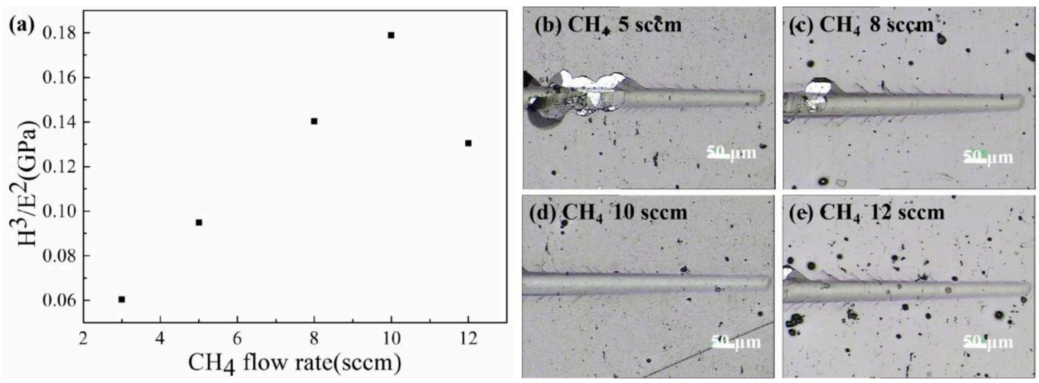

Figure 7. (**a**) The value of H^3/E^2 and (**b**–**e**) scratch test as a function of CH_4 flow rate.

3.3. Tribological Behavior

3.3.1. Against Steel Ball

The COF curves of sample 2 to 5 against the steel ball are given in Figure 8a. The average COF of the samples firstly reduces as the CH_4 flow rate increases during deposition and reaches the minimum average COF value of 0.1665 in sample 4, which is deposited under a CH_4 flow rate of 10 sccm. Then, the average COF increases slightly with a further increase in CH_4 flow rate and reaches 0.1792 when the CH_4 flow rate is at 12 sccm. The average COF value of sample 4 is lower than that reported by other authors [22,27,28]. The dense microstructure and existence of the amorphous C and TiC phase may lubricate the contact area during sliding against the steel ball and lower the COF. It is observed in Figure 8a that the time of the steady stage [29] of COF in sample 4 and 5 is hardly identical and is longer than in sample 2 and 3. However, the lubricative property of sample 5 is still maintained after the steady stage, and the COF value fluctuates from 0.18 to 0.28 in this period. The wear rates of sample 4 and 5 are 2.43×10^{-6} mm^3/N·m and 4.12×10^{-6} mm^3/N·m against the steel ball, respectively, as shown in Table 2. This result indicates that the wear rate is not in accordance with the wear life in sample 4 and 5, but in agreement with the result of the H^3/E^2 value. It is worth noticing that the wear debris of sample 4 contains about 10 at.% Fe and that of sample 5 only contains 8 at.% Fe, measured by EDS. It is obviously revealed that sample 4 is subjected to serious adhesion wear [30] when sliding against the steel ball. It explains why sample 4 exhibits a shorter life span and lower wear rate than sample 5.

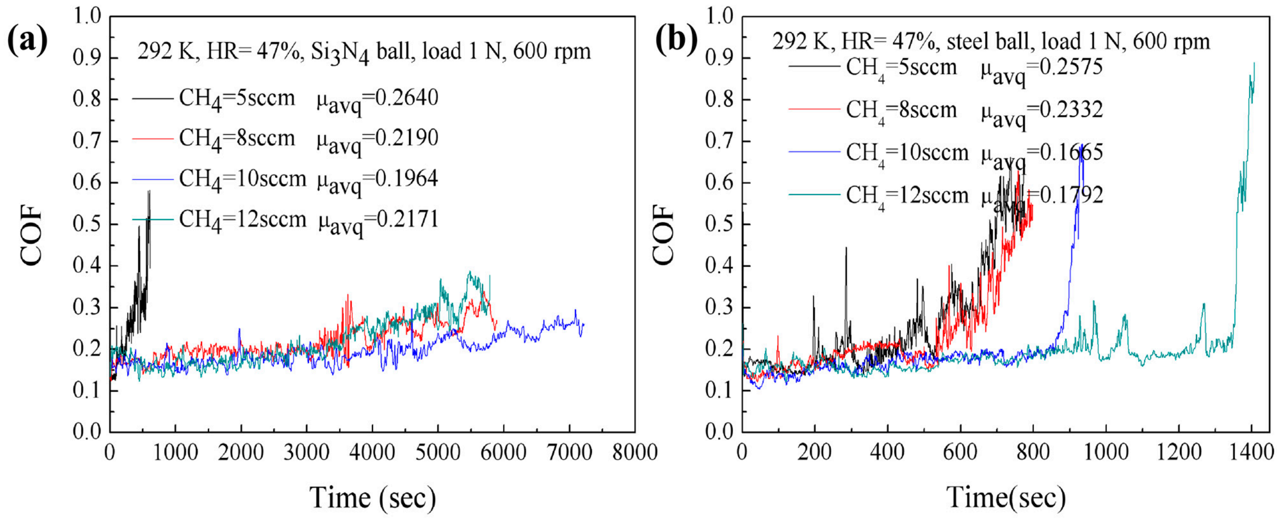

Figure 8. The COF curves of the films: (**a**) against steel ball, (**b**) against Si_3N_4 ball.

Table 2. The wear rate of the films deposited.

Samples	**CH_4 (sccm)**	**Wear Rate (10^{-6} mm^3/N·m)**	
		Against Steel Ball	**Against Si_3N_4 Ball**
2	5	3.35	3.52
3	8	5.90	2.33
4	10	2.43	2.08
5	12	4.12	5.39

3.3.2. Against Si_3N_4 Ball

Figure 8b shows typical COF curves corresponding to the samples with CH_4 flow rates ranging from 5 to 12 sccm against with the Si_3N_4 ball. Sample 2 deposited under a CH_4 flow rate of 5 sccm presents poor tribological properties, including high COF and a short life span, because of the less amorphous carbon, loose microstructure and low hardness. The wear rate of sample 2 is 3.52×10^{-6} mm^3/N·m as shown in Table 2. The COF and life span for sample 3 and 5 are almost identical, approximately reaching 0.22 and 60,000 cycles, respectively. However, their wear rates are 2.33×10^{-6} mm^3/N·m and 5.39×10^{-6} mm^3/N·m, respectively. However, sample 4 possessed the minimum average COF value of 0.1964 and reaches 72,000 cycles against the Si_3N_4 ball throughout the test duration. The wear rate of sample 4 is 2.08×10^{-6} mm^3/N·m, which is lower than that of other samples. These results indicate that the sample deposited under a CH_4 flow rate of 10 sccm possesses optimal tribological behavior against the Si_3N_4 ball. Low or high C content in the samples shows certain wear problems. It is explained that the sample deposited under a CH_4 flow rate of 10 sccm possesses a dense microstructure, high hardness and good resistance to plastic deformation. This result is consistent with the conclusion of H^3/E^2 mentioned above.

3.3.3. Comparative Study

All the samples make the COF slightly lower against the steel ball than the Si_3N_4 ball except sample 3, as shown in Figure 8. It is suggested that TiCN films present better lubricative properties when against low-hardness counterparts than high-hardness counterparts. This result can be attributed to the fact that the translation layer formed during the sliding tests is softer by contrast with the Si_3N_4 ball. In addition, it is easily found that sample 4 deposited under a CH_4 flow rate of 10 sccm shows excellent friction properties, not only against the steel ball but also against the Si_3N_4 ball, resulting from the existence of a dense and globular microstructure, appropriate amount of amorphous carbon and TiC phase. Moreover, the life span of all the samples is longer against the Si_3N_4 ball than against the steel ball. It can be explained that the steel ball is easily oxidated by a tribo-chemical reaction [30,31] compared with the Si_3N_4 ball. The wear rate of the films is given in Table 2 against the Si_3N_4 ball and steel ball. The difference in wear rate for sample 2 between sliding against the steel ball and the Si_3N_4 ball is neglected due to the short time of the sliding test. The wear rate of other samples has an obvious difference against the Si_3N_4 ball and steel ball. It is worth noticing that wear rates for sample 3 and 4 are 5.905×10^{-6} $mm^3/N{\cdot}m$ and 2.43×10^{-6} $mm^3/N{\cdot}m$, respectively, against the steel ball. However, the wear rate of sample 5 is 4.12×10^{-6} $mm^3/N{\cdot}m$ against the steel ball, which is about 1.27×10^{-6} $mm^3/N{\cdot}m$ lower than against the Si_3N_4 ball. In Figures 6 and 7, it is easily found that the hardness and H^3/E^2 values of sample 3 and 4 are higher than that of sample 5. Therefore, the hard samples present poor wear resistance when sliding against the steel ball. On the contrary, the samples with relatively low hardness exhibit better wear resistance against the steel ball than against the Si_3N_4 ball. These results could be attributed to the wear rate, which is closely related to the difference in the hardness between the film and its counterpart. When the difference is small, the wear resistance is good.

4. Conclusions

TiCN films were deposited on stainless steel and silicon (100) substrates under different CH_4 flow rates by DCMS. The composition, microstructure and hardness of the films were studied, and the tribological behavior of the Ti-TiN-TiCN films sliding against a steel ball and a Si_3N_4 ball in air had already been investigated in detail. The main results can be summarized as:

1. The TiCN films displayed a gradual change in microstructure from loose and sharp pyramid-like to dense and globular nanostructure, with an increasing CH_4 flow rate. The TiC phase was found in the TiCN film deposited at 10 sccm CH_4 flow rates. Along with the rise in CH_4 flow rates, the content of amorphous carbon raised. The grain size calculated by Scherrer's formula decreased from 19.3 nm to 4.1 nm as the CH_4 flow rate increased.
2. The TiCN film deposited at 8 sccm CH_4 flow rates had an optimal value of hardness. However, the value of H^3/E^2 of the film deposited under a 10 sccm CH_4 flow rate was the uppermost value.
3. The COF of the films firstly decreased and then increased by adding a CH_4 flow rate while sliding against both the steel and the Si_3N_4 ball. The TiCN film obtained under a 10 sccm CH_4 flow rate exhibited excellent tribological behaviors against both the steel ball and the Si_3N_4 ball.
4. The films presented lower COF and shorter life span against the steel ball than the Si_3N_4 ball. However, the high hard films exhibited better wear resistance against the Si_3N_4 ball than the steel ball and vice versa.

Due to the films deposited at room temperature in this work, they may be limited to applications in high-temperature cutting tools. Therefore, the mechanical and tribological properties at high temperature of Ti/TiN/TiCN triple-layer films should be studied in the future.

Author Contributions: Conceptualization, methodology, software, validation, formal analysis, investigation, resources, data curation, writing—original draft preparation, writing—review, Y.L. (Yanhong Lyu) and J.Z.; editing, J.Z., X.D., H.S., Q.Z., Y.L. (Yang Liu) and Y.L. (Yanhong Lyu); supervision, Y.L. (Yanhong Lyu); project administration, Y.L. (Yanhong Lyu); funding acquisition, Y.L. (Yanhong Lyu). All authors have read and agreed to the published version of the manuscript.

Funding: This research was funded by Provincial Natural Science Foundation of Hunan, grant number 2021JJ40140 and the Scientific Research Fund of Hunan Provincial Education Department, grant number Grant No. 21B0812.

Data Availability Statement: Data is contained in the article.

Acknowledgments: This research also appreciates the help and guidance by Junying Hao.

Conflicts of Interest: The authors declare no conflict of interest.

References

1. Feng, W.R.; Zhou, H.; Yang, S.Z. Nano-indentation and wear-resistance behaviors of TiCN films by pulsed plasma on cemented carbide cutting tool. *Mater. Sci. Eng. A* **2010**, *527*, 4767–4770. [CrossRef]
2. Zhang, F.; He, J.; Chen, K.; Qin, Y.; Li, C.; Yin, F. Microstructure evolution and mechanical properties of TiCN-Cr nano/micro composite coatings prepared by reactive plasma spraying. *Appl. Surf. Sci.* **2018**, *427*, 905–914. [CrossRef]
3. Kumar, T.S.; Jebaraj, A.V.; Shankar, E.; Tamiloli, N.; Sivakumar, K. Metallurgical and mechanical characterization of TiCN/TiAlN and TiAlN/TiCN bilayer nitride coatings. *Surf. Inter.* **2019**, *15*, 256–264.
4. Cheng, Y.H.; Browne, T.; Heckerman, B. Influence of CH_4 fraction on the composition, structure, and internal stress of the TiCN coatings deposited by LAFAD technique. *Vacuum* **2010**, *85*, 89–94. [CrossRef]
5. Hsieh, J.; Li, C.; Wu, W.; Tan, A. Synthesis of TiC, N, O coatings by unbalanced magnetron sputtering. *J. Mater. Process. Technol.* **2003**, *140*, 662–667. [CrossRef]
6. Balaceanu, M.; Braic, M.; Braic, V.; Pavelescu, G. Properties of arc plasma deposited TiCN/ZrCN superlattice coatings. *Surf. Coat. Technol.* **2005**, *200*, 1084–1087. [CrossRef]
7. Podchernyaeva, I.A.; Lavrenko, V.A.; Umanskii, A.P.; Koror, A.A.; Timofeeva, I.I.; Yuga, A.I. Electric-spark alloying of structural alloys with a composite based on TiCN-AlN. *Powder Metall. Met. Ceram.* **2000**, *39*, 232–238. [CrossRef]
8. Lackner, J.M.; Waldhauser, W.; Ebner, R.; Bakker, R.J. Chemistry and microstructure of PLD Ti, AlCxN1-x coatings deposited at room temperature. *Appl. Phys. A* **2004**, *79*, 1469–1471. [CrossRef]
9. Bemporad, E.; Pecchio, C.; De Rossi, S.; Carassiti, F. Characterization and hardness modelling of alternate TiN/TiCN multilayer cathodic arc PVD coating on tool steel. *Surf. Coat. Technol.* **2001**, *146*, 363–370. [CrossRef]
10. Huber, P.; Manova, D.; Mandl, S.; Rauschenbach, B. Formation of TiN, TiC and TiCN by metal plasma immersion ion implantation and deposition. *Surf. Coat. Technol.* **2003**, *174*, 1243–1247. [CrossRef]
11. Zheng, J.Y.; Hao, J.Y.; Liu, X.Q.; Gong, Q.Y.; Liu, W.M. TiN/TiCN Multilayer Films Modified by Argon Plasma Treatment. *Appl. Surf. Sci.* **2013**, *280*, 764. [CrossRef]
12. Zheng, J.Y.; Ren, X.D.; Hao, H.Y.; Li, A.; Liu, W.M. Carbon nanohoops as attractive toughening and lubricant agents in TiN porous films. *Appl. Surf. Sci.* **2017**, *393*, 60–66. [CrossRef]
13. Wang, Q.; Jin, X.; Zhou, F. Comparison of mechanical and tribological properties of CrBN coatings modified by Ni or Cu incorporation. *Friction* **2022**, *10*, 516. [CrossRef]
14. Serro, A.P.; Completo, C.; Colaço, R.; dos Santos, F.; Lobato da Silva, C.; Cabral, J.M.S.; Araújo, H.; Pires, E.; Saramago, B. A comparative study of titanium nitrides, TiN, TiNbN and TiCN, as coatings for biomedical applications. *Surf. Coat. Technol.* **2009**, *203*, 3701–3707. [CrossRef]
15. Yang, Y.L.; Yao, W.M.; Zhang, H.Z. Phase constituents and mechanical properties of laser in-situ synthesized TiCN/TiN composite coating on Ti-6Al-4V. *Surf. Coat. Technol.* **2010**, *205*, 620–624. [CrossRef]
16. Canteli, J.A.; Cantero, J.L.; Marín, N.C.; Gómez, B.; Gordo, E.; Miguélez, M.H. Cutting performance of TiCN-HSS cermet in dry machining. *J. Mater. Process. Technol.* **2010**, *210*, 122–128. [CrossRef]
17. Guruvenket, S.; Li, D.; Klemberg-Sapieha, J.E.; Martinu, L.; Szpunar, J. Mechanical and tribological properties of duplex treated TiN, nc-TiN/a-SiNx and nc-TiCN/a-SiCN coatings deposited on 410 low alloy stainless steel. *Surf. Coat. Technol.* **2009**, *203*, 2905–2911. [CrossRef]
18. Su, Y.L.; Kao, W.H. Tribological behavior and wear mechanisms of TiN/TiCN/TiN multilayer coatings. *J. Mater. Eng. Perform.* **1998**, *7*, 601–612. [CrossRef]
19. Eizenberg, M.; Littau, L.; Ghanayem, S.; Liao, M.; Mosely, R.; Sinha, A.K. Chemical vapor deposited TiCN: A new barrier metallization for submicron via and contact applications. *J. Vac. Sci. Technol. A* **1995**, *13*, 590–595. [CrossRef]
20. Klemberg-Sapieha, J.E.; Jedrzejowski, P.; Martinu, L. Mechanical and optical characteristics of superhard nanocomposite TiN/a-Si_3N_4 and TiCN/a-SiCN coatings produced by PECVD. *J. Superhard Mater.* **2007**, *29*, 147–152. [CrossRef]
21. Escobar-Alarcón, L.; Camps, E.; Romero, S.; Muhl, S.; Camps, I.; Haro-Poniatowski, E. TiCN thin films grown by reactive crossed beam pulsed laser deposition. *Appl. Phys. A Mater. Sci. Process.* **2010**, *101*, 771–775. [CrossRef]
22. Deng, J.G.; Braun, M.; Gudowska, I. Properties of TiCN coatings prepared by magnetron sputtering. *J. Vac. Sci. Technol. A* **1994**, *12*, 733–736. [CrossRef]
23. Rabiei, M.; Palevicius, A.; Monshi, A.; Nasiri, S.; Vilkauskas, A.; Janusas, G. Comparing Methods for Calculating Nano Crystal Size of Natural Hydroxyapatite Using X-Ray Diffraction. *Nanomaterials* **2020**, *10*, 1627. [CrossRef] [PubMed]

24. Klug, H.P.; Alexander, L.E. *X-ray Diffraction Procedures for Polycrystalline and Amorphous Materials*; Wiley-Interscience: New York, NY, USA, 1974.
25. Morant, C.; Prieto, P.; Forn, A.; Picas, J.A.; Elizalde, E.; Sanz, J.M. Hardness enchancement by CN/TiCN/TiN multilayer films. *Surf. Coat. Technol.* **2004**, *180*, 512–518. [CrossRef]
26. Caicedo, J.C.; Amaya, C.; Yate, L.; Gómez, M.E.; Zambrano, G.; Alvarado-Rivera, J.; Muñoz-Saldaña, J.; Prieto, P. TiCN/TiNbCN multilayer coatings with enhanced mechanical properties. *Appl. Surf. Sci.* **2010**, *256*, 5898–5904. [CrossRef]
27. Zukerman, I.; Raveh, A.; Landau, Y.; Weiss, R.; Shneck, R.; Shneor, Y.; Kalman, H.; Klemberg-Saphieha, J.E.; Martinu, L. Tribological properties of duplex treated TiN/TiCN coatings on plasma nitrided PH15-5 steel. *Surf. Coat. Technol.* **2007**, *201*, 6171–6175. [CrossRef]
28. Polcar, T.; Novák, R.; Široký, P. The tribological characteristics of TiCN coating at elevated temperatures. *Wear* **2006**, *260*, 40–49. [CrossRef]
29. Mo, J.L.; Zhu, M.H. Sliding tribological behaviors of PVD CrN and AlCrN coatings against Si_3N_4 ceramic and pure titanium. *Wear* **2009**, *267*, 874–881. [CrossRef]
30. Mo, J.L.; Zhu, M.H.; Lei, B.; Leng, Y.X.; Huang, N. Comparison of tribological behaviours of AlCrN and TiAlN coatings deposited by physical vapor deposition. *Wear* **2007**, *263*, 1423–1429. [CrossRef]
31. Hager, C.H., Jr.; Sanders, J.; Sharma, S.; Voevodin, A. Gross slip fretting wear of CrCN, TiAlN, Ni, and CuNiIn coatings on Ti6Al4V interfaces. *Wear* **2007**, *263*, 430–443. [CrossRef]